

Betrayed by Attention: A Simple yet Effective Approach for Self-supervised Video Object Segmentation

Shuangrui Ding^{1†} Rui Qian^{1†} Haohang Xu² Dahua Lin^{1,3} Hongkai Xiong²

¹The Chinese University of Hong Kong ²Shanghai Jiao Tong University

³Shanghai Artificial Intelligence Laboratory

{dsr1212, qr021}@ie.cuhk.edu.hk

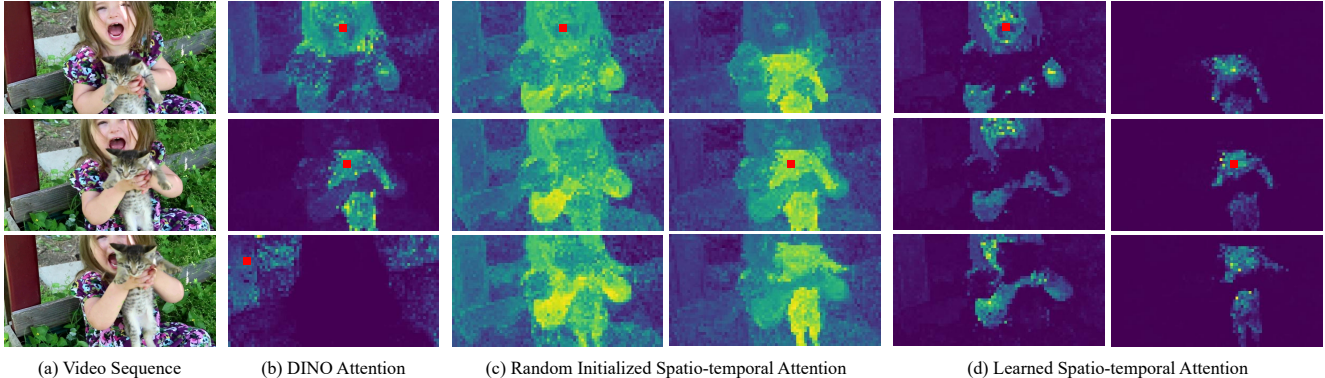


Figure 1. Attention leaks the object’s position! We visualize the self-attention maps of different queries (red prompt) from the video sequence (a). The frame-wise DINO attention maps (b) highlight image regions corresponding to the queried object. A randomly initialized spatio-temporal Transformer block on top of DINO produces noisy spatio-temporal attention maps (c) that coarsely track objects over time. Our method diminishes noise in the learned spatio-temporal attention maps (d) which derive temporally coherent object segmentation.

Abstract

In this paper, we propose a simple yet effective approach for self-supervised video object segmentation (VOS). Our key insight is that the inherent structural dependencies present in DINO-pretrained Transformers can be leveraged to establish robust spatio-temporal correspondences in videos. Furthermore, simple clustering on this correspondence cue is sufficient to yield competitive segmentation results. Previous self-supervised VOS techniques majorly resort to auxiliary modalities or utilize iterative slot attention to assist in object discovery, which restricts their general applicability and imposes higher computational requirements. To deal with these challenges, we develop a simplified architecture that capitalizes on the emerging objectness from DINO-pretrained Transformers, bypassing the need for additional modalities or slot attention. Specifically, we first introduce a single spatio-temporal Trans-

former block to process the frame-wise DINO features and establish spatio-temporal dependencies in the form of self-attention. Subsequently, utilizing these attention maps, we implement hierarchical clustering to generate object segmentation masks. To train the spatio-temporal block in a fully self-supervised manner, we employ semantic and dynamic motion consistency coupled with entropy normalization. Our method demonstrates state-of-the-art performance across multiple unsupervised VOS benchmarks and particularly excels in complex real-world multi-object video segmentation tasks such as DAVIS-17-Unsupervised and YouTube-VIS-19. The code and model checkpoints will be released at <https://github.com/shvdiwnkozbw/SSL-UVOS>.

1. Introduction

Representing the visual scene with objects as the basic elements has been long acknowledged as a core cognitive capability of an intelligent agent. In the realm of computer vision, Video Object Segmentation (VOS) tasks require a model to segment and track specified objects within a video

† Equal contribution.

sequence, striving to emulate this foundational function. This task holds significant importance in various real-world vision systems, including but not limited to, autonomous driving [18] and surveillance security [47]. However, traditional methods for VOS [6, 49] typically follow a fully supervised paradigm and entail substantial costs for obtaining pixel-level per-frame annotations. This factor significantly limits their feasibility for large-scale applications. Thus, the researchers turn their attention to self-supervised learning [8, 10, 11, 21, 51, 52], a more efficient approach that leverages unlabeled data.

Despite its promising potential, self-supervised VOS poses significant challenges. Firstly, previous methods tend to incorporate additional signals such as optical flow [37, 66, 68], or depth cues [15, 27], to furnish object-related clues. However, these auxiliary signals within videos can often be difficult to extract, thus compromising their availability. Secondly, most existing models [1, 53, 73] adopt slot attention [39] to parse the frame into objects. Nevertheless, the requirement for a predefined quantity of learnable slot queries limits its adaptability to in-the-wild data, especially when the number of objects is unknown. Additionally, the use of either external modality or slot attention imposes an extra computational burden on the model. To address these limitations, we recall the recent self-supervised learning technique DINO [7, 46], which demonstrates emerging objectness in the attention maps of pre-trained Vision Transformer (ViT) [13]. As depicted in Fig. 1(b), DINO attention maps encode spatial dependencies between diverse patches. These dependencies present different patterns for various objects, providing abundant cues for object segmentation. This phenomenon motivates us with an intriguing possibility: Can we utilize the object-aware attributes of DINO to learn robust spatio-temporal dependencies and thereby produce coherent object segmentations in videos?

In this paper, we delve into the potential of this idea with a simple architecture. Based on DINO pretrained ViT, we introduce a single spatio-temporal Transformer block to process frame-wise DINO features and calculate spatio-temporal attention maps. Remarkably, these attention maps in Fig. 1(c) showcase the ability to coarsely discriminate and track object parts even with random initialization. This observation leads us to consider attention maps as valuable indicators that reveal the positions likely to be associated with the same object over time. Then, we encourage both semantic and motion alignment among patches belonging to the same object while distinguishing those from different objects in a fully self-supervised manner. The training significantly diminishes noise in the learned spatio-temporal dependencies as displayed in Fig. 1(d). Building on this insight, in inference, we directly apply Hierarchical Clustering [26] to these spatio-temporal attention maps to de-

rive object segmentation masks within a sequence. Interestingly, this naive clustering method yields unexpectedly competitive results. And the effectiveness of this approach can be attributed to clustering on the spatio-temporal attention maps, instead of frame-by-frame feature clustering as in slot attention. This fundamentally ensures the temporal coherence of produced segmentations and guarantees the object’s permanence.

In summary, our proposed method offers three distinct advantages: (1) Our approach solely requires RGB frames and operates entirely under self-supervision without the need for external modality. This characteristic renders our method highly accessible and adaptable in real-world scenarios; (2) The architecture is remarkably simple and systematically efficient. We only introduce a single learnable Transformer block and harness a parameter-free clustering algorithm to discover the objects. It facilitates easy generalization to novel scenes, without the constraints imposed by slot attention; (3) Our method achieves state-of-the-art results across a bunch of unsupervised VOS benchmarks, including single object segmentation tasks like DAVIS-16 [48], SegTrack-v2 [32], FBMS-59 [44], as well as multi-object segmentation tasks such as MOVi-E [19], DAVIS-17-Unsupervised [50], and YouTube-VIS-19 [67]. Notably, we surpass the previous state-of-the-art method, TimeT [54], by 6.6% on YTVIS-19 and by 6.1% on DAVIS-17 in terms of the FG-ARI metric.

2. Related Work

Video Object Segmentation aims to segment objects coherently in a video sequence [2, 6, 14, 17, 23, 25, 29, 34, 41, 45, 49]. In video object segmentation (VOS), there are two prevalent protocols for evaluating the learned models: Semi-supervised VOS and Unsupervised VOS. In semi-supervised VOS, the algorithm is provided with the object masks in the first frame, and required to track them in subsequent frames. In contrast, unsupervised VOS aims to identify and segment salient objects from the background without any specific reference. In this paper, we focus on the more challenging unsupervised VOS setting without using any kind of manual annotations in either training or inference. Recently, there emerges a line of self-supervised algorithms for unsupervised VOS [9, 27, 35, 59, 63, 66, 68, 69, 71]. CIS [68] facilitates fully unsupervised motion segmentation, discarding object mask supervision during training. By formulating a min-max game of mutual information, the generator is motivated to create segmentations that effectively distinguish foreground objects from the background. AMD [38] minimizes the warping synthesis error to train appearance and motion pathways without any supervision. GWM [9] uses a single RGB image as input with optical flow acting as supervision to highlight moving areas. MG [66] and OCLR [64] solely leverage optical flow

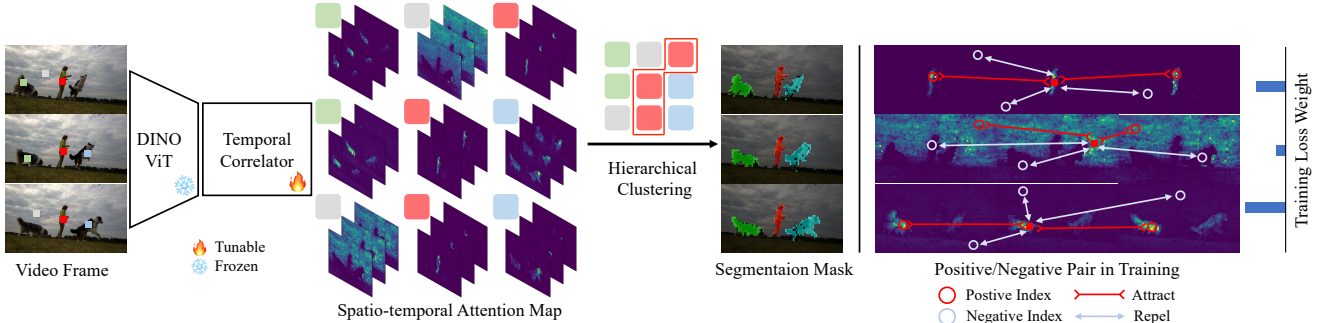


Figure 2. Our architecture overview. Given the video frames and a DINO pretrained Transformer, we first use a temporal correlator to construct the spatio-temporal correspondence. We then utilize these attention maps as a clustering metric and apply hierarchical clustering across all frames to generate segmentation masks in one shot. During training, for each patch, we sample a positive/negative set and assign an importance weight based on its corresponding attention map. We promote alignment within the positive set while differentiating the representations from the negative set. The final loss, computed with importance weights, only trains the temporal correlator with the DINO ViT remaining frozen.

as input to generate object-centric layered representations, with each layer indicating a potential object. Despite the impressive performance of state-of-the-art self-supervised VOS methods [1, 53, 54] in discovering single objects, they still face limitations when it comes to solving multi-object discovery tasks. In contrast, by leveraging the rich object cues in attention maps, our method can not only pick out the most salient foreground areas for single object discovery but also discern multiple objects in real-world scenarios.

Self-supervised Spatio-temporal Correspondence learning usually leverages free temporal supervision signals in videos to learn representations that facilitate accurate pixel or object tracking across space and time [4, 7, 22, 24, 29, 30, 36, 58, 60, 65]. Vondrick et al. [58] employ the natural temporal color coherence to train a colorization model on grayscale videos, thereby establishing fine-grained correspondence between current and future frames. CRW [24] presents a self-supervised learning approach for dense correspondence in raw videos. It uses space-time graph-based random walks and cycle consistency to implicitly supervise chains of comparisons. Hu et al. [22] independently learn semantics and temporal correspondence from two pathways and fuse them at a later stage. UME [33] respectively designs short-term appearance and long-term semantic consistency to learn generalizable correspondence. Taking a step further by integrating high-level semantics with low-level temporal correlation, SMT [53] develops two-stage slot attention to establish dense correspondence with more emphasis on foreground objects. In this work, we explicitly initialize the spatio-temporal correspondence on top of the DINO pretrained Transformer. This initialization effectively guides the learning process with a self-supervised pixel-level consistency.

Object-aware DINO Features have shown efficacy in object localization tasks, particularly in image domain [5, 20,

42, 56, 61, 72, 74]. DINO’s original paper [7] reveals that the learned representations and attention maps carry substantial object cues that can be harnessed for object discovery. The groundbreaking work, LOST [56], utilizes these features from DINO to perform object segmentation by constructing a graph wherein objects are segmented using the inverse degrees of nodes. TokenCut [62] employs DINO features for applying the Normalized Cut algorithm [55], thereby obtaining foreground segments in an image. Motivated by the successful application of DINO features in image settings, recent works have expanded their use to video segmentation tasks [1, 53, 54, 62]. SMT [53] utilizes the rich semantics and correspondence cues in the DINO features to provide a reliable reference for object decomposition in consecutive frames. TimeT [54] introduces a feature forwarding process to propagate dense DINO features across time and establish temporal consistency. SOLV [1] applies invariant slot attention on DINO features to distill object-centric representations and merge similar slots into candidate objects. Most of the existing works focus on leveraging DINO feature vectors for optimization and adaptation to videos. While in our work, we lay more emphasis on the self-attention maps. We extend the frame-wise DINO attention maps to spatio-temporal domain, which explicitly encode space-time structural dependencies and guide temporally coherent object discovery in videos.

3. Method

The aim of this paper is to develop a self-supervised approach for video object segmentation without relying on either other modalities [64] or slot attention [39]. We begin with an initial exploration of clustering the frame-wise attention maps and features from DINO in Section 3.1, observing that the attention map is remarkably more effective for VOS task than the features. Motivated by this, in Sec-

Clustering Metric	Cosine similarity		KL divergence		
	F		A	A_v	\tilde{A}_v
DAVIS-16	47.4		60.3	51.1	75.4
DAVIS-17	14.7		26.7	20.9	39.2

Table 1. Preliminary video object segmentation results using varying clustering metrics. F represents features pretrained with DINO. A denotes per-frame attention maps from DINO, while A_v and \tilde{A}_v denote spatio-temporal attention maps produced by a randomly initialized and a final learned temporal correlator respectively, on top of DINO. The IoU (\mathcal{J} score) is reported for both DAVIS-16 and DAVIS-17-Unsupervised datasets.

tion 3.2, we straightforwardly construct the spatio-temporal correspondence in the form of self-attention, and directly apply clustering on these spatio-temporal structural dependencies for video segmentation tasks. Our main pipeline is illustrated in Fig. 2. To train our proposed module, we propose a dual semantic and motion consistency protocol coupled with entropy normalization, as detailed in Section 3.3.

3.1. Preliminary on DINO Attention Maps

The self-supervised ViT, as achieved by DINO [7], has exhibited a rich emergence of objectness in the attention maps. To elucidate this, we visualize the self-attention map from the final Transformer block of the DINO pretrained ViT-S/8 as a representative. As illustrated in Fig. 1(b), an image patch exhibits a high degree of attention dependencies with patches that reside within the same object. Conversely, image patches of distinct objects tend to manifest different attention distributions. Encouraged by this observation, we pose the following question: could it be possible to directly harness these attention maps to achieve object discovery without relying on annotations?

In response to this question, we conduct a straightforward initial exploration with these attention maps. We denote the attention map of the last Transformer Block as $A \in \mathbb{R}^{HW \times HW}$ and its output features $F \in \mathbb{R}^{HW \times C}$, where H , W and C respectively denote the height, width, and channel dimension of the feature map¹. For an intuitive comparison, we apply unsupervised clustering on both attention maps A and features F to yield the object segmentation masks. For the detailed procedure, please refer to the Sec. 3.2. Then, we report frame-wise evaluation results on the video object segmentation datasets DAVIS-16 [48] and DAVIS-17-Unsupervised [50] in Table 1. Interestingly, we observe that the attention maps significantly excel in decoupling object components compared to features, exhibiting an improvement of over **10** points on both datasets in terms of IoU. We surmise this is because the attention maps pre-

¹Here we omit the **CLS** token, and average the multi-head attention along the head dimension.

serve intact correspondences, which are more suitable for fine-grained tasks such as object grouping and discrimination. Therefore, creating spatio-temporal structural dependencies that expand beyond spatial DINO attention maps appears promising for video object segmentation tasks.

3.2. Our Simple Architecture for VOS

Motivated by the frame-wise preliminary result, we introduce a temporal correlator instantiated with a spatio-temporal Transformer block [3] on top of the DINO pretrained ViT backbone, to extend the self-attention calculation to the spatio-temporal domain. Specifically, given the frame-wise DINO features $\{F_1, \dots, F_T\}$ of T frames, we process them through a spatio-temporal Transformer block Φ_{st} as follows:

$$\{\tilde{F}_1, \dots, \tilde{F}_T\} = \Phi_{st}(F_1 + \text{pe}_1, \dots, F_T + \text{pe}_T), \quad (1)$$

where pe represents learnable temporal positional embeddings. The resulting temporally fused features $\tilde{F}_t \in \mathbb{R}^{HW \times C}$ maintain the same dimension as the input. It is important to note that Φ_{st} also produces an intermediate output, the spatio-temporal attention maps $A_v \in \mathbb{R}^{THW \times THW}$, where $A_v[i]$ signifies the correlations between the i -th position and all spatio-temporal patches. In this way, we establish spatio-temporal structural dependencies beyond frame-wise DINO features and have the potential to improve object permanence across the entire time span.

Since $A_v[i] \in \mathbb{R}^{THW}$ is a proximity distribution that describes the structural dependencies between the i -th patch and all other positions, we adopt symmetric KL divergence to measure the distance $\mathcal{M} \in \mathbb{R}^{THW \times THW}$ between any two patches as:

$$\mathcal{M}[i, j] = \mathcal{D}_{KL}(A_v[i] \parallel A[j]) + \mathcal{D}_{KL}(A_v[j] \parallel A_v[i]), \quad (2)$$

where \mathcal{D}_{KL} denotes KL divergence. Based on this distance matrix \mathcal{M} , we then apply Hierarchical Clustering [26] to obtain the object segmentation masks. Please consult our appendix for an detailed implementation of the hierarchical clustering algorithm. In this way, we iteratively merge THW patches into K centroids $A_c \in \mathbb{R}^{K \times THW}$. Since each centroid likely represents the spatial distribution of an object, we consider the cluster assignments as potential candidates for the object segmentation mask. Specifically, we calculate the KL divergence distance between the A_v and A_c as $D \in \mathbb{R}^{THW \times K}$, and use argmin operation to produce the cluster assignments Z within the video sequence:

$$Z = \text{argmin}(D, \text{dim}=1) \in \{1, \dots, K\}^{THW}. \quad (3)$$

Then, we employ a bipartite matching mechanism, following the standard evaluation protocol in DAVIS-17 Challenge [50], to match the predicted masks with ground truth for evaluation.

There are two noteworthy aspects in our clustering stage. First, in the clustering process, we only set a distance threshold hyper-parameter without specifying the number of cluster centroids and the hierarchical clustering algorithm can adaptively generate different numbers of clusters according to the complexity of the video. Second, our reference to the entire spatio-temporal distribution enables coherent object segmentation across multiple frames. As a result, the generated segmentation masks effortlessly track corresponding objects over time without extra association procedures.

3.3. Training

Noticing that even a randomly initialized attention map A_v shown in Figure 1(c), exhibits an initial ability to differentiate parts and track objects over time, we leverage these maps as indicators for positive and negative sets sampling. Mathematically, given the attention maps $A_v \in \mathbb{R}^{THW \times THW}$, we first reshape A_v into shape $THW \times T \times HW$ then use top-k operation to retrieve K_p position indexes in each frame with highest attention scores:

$$I_p = \text{top-k}(\text{reshape}(A_v), K_p, \text{dim}=-1). \quad (4)$$

In this way, we obtain a position index set $I_p \in \mathbb{R}^{THW \times T \times K_p}$, which represents positions potentially associated with the same object as the i -th patch. The reshape operation ensures that we consistently extract the same number of patches in each frame. This, in turn, guarantees effective object tracking within consecutive frames and promotes consistent temporal correspondence learning. Similarly, we perform this operation to find K_n positions in each frame with the lowest attention scores $I_n \in \mathbb{R}^{THW \times T \times K_n}$. Each $I_n[i]$ represents positions least likely to belong to the same object as the i -th patch. After obtaining the positive and negative index sets, we apply self-supervised correspondence learning in two aspects: semantic consistency and dynamic motion consistency.

Semantic consistency. Intuitively, we take the temporally fused features $F_v = \{\tilde{F}_1, \dots, \tilde{F}_T\} \in \mathbb{R}^{THW \times C}$ as the semantic representation. We promote the semantic alignment between the features of the same object and distinguish features from different objects. Given the i -th patch, we first refer to the positive pair indexes $I_p[i]$ in Eq. 4 to gather the features that are likely from the same object. Then we calculate the cosine distance between the query feature and all positive feature vectors, and produce the distance matrix $\mathcal{S}_p[i] \in \mathbb{R}^{TK_p}$. Similarly, we gather distinct features using $I_n[i]$, and form negative distance matrix $\mathcal{S}_n[i]$. We employ a simple margin loss to enforce higher consistency between corresponding object areas:

$$\mathcal{L}_s[i] = \sum_{j=1}^{TK_p} \sum_{k=1}^{TK_n} \max(\mathcal{S}_p[i, j] - \mathcal{S}_n[i, k] + \lambda_1, 0), \quad (5)$$

where λ_1 is the margin hyper-parameter.

Dynamic motion consistency. Regarding dynamic motions, rather than calculating optical flow, inter-frame feature correlations, or latent cost volumes as motion representations, we turn to readily accessible attention maps A_v . These maps exhibit spatio-temporal correlations of specific patches, serving as an effective latent representation of temporal dynamics. Therefore, it is feasible to directly employ these attention maps to bolster motion consistency between corresponding objects. Similar to the semantic consistency learning, given the attention map of i -th patch $A_v[i]$ as query, we also leverage the positive (negative) pair indexes $I_p[i]$ ($I_n[i]$) to gather the attention maps of the corresponding (distinct) objects. Then we calculate the symmetric KL divergence as in Eq. 2 between the query and all positive (negative) attention maps, obtaining the distance matrix $\mathcal{M}_p[i] \in \mathbb{R}^{TK_p}$ and $\mathcal{M}_n[i] \in \mathbb{R}^{TK_n}$. We utilize the same margin loss for optimization, with λ_2 as the margin hyper-parameter:

$$\mathcal{L}_m[i] = \sum_{j=1}^{TK_p} \sum_{k=1}^{TK_n} \max(\mathcal{M}_p[i, j] - \mathcal{M}_n[i, k] + \lambda_2, 0). \quad (6)$$

Overall objectives. Besides, we evaluate the importance of each spatio-temporal patch and lay more emphasis on the informative regions. Formally, we employ the entropy of the attention maps as a measure of the information content within each patch:

$$e[i] = \sum_{k=1}^{THW} -A_v[i, k] \log A_v[i, k], \quad (7)$$

with $e[i]$ denoting the entropy of i -th patch. A higher entropy value indicates more ambiguous spatio-temporal correlations, which provide less information. Hence, we perform softmax normalization on the reversed entropy to produce the importance weight w for each patch as:

$$w[i] = \frac{\exp(-e[i])}{\sum_{j=1}^{THW} \exp(-e[j])}. \quad (8)$$

Then, the overall learning objectives on semantic and motion consistency can be formulated as the weighted summation over all spatio-temporal patches:

$$\mathcal{L} = \sum_{i=1}^{THW} w[i](\mathcal{L}_s[i] + \mathcal{L}_m[i]). \quad (9)$$

Since we only introduce one additional temporal correlator and an entirely parameter-free clustering strategy, we exclusively tune a single standard spatio-temporal Transformer block with the pretrained ViT frozen throughout the training process. This exceptionally simple method not only maintains a minimal number of learnable parameters but also yields remarkable results in video object segmentation.

4. Experiments

4.1. Datasets

For training, we adopt the challenging video dataset YouTube-VIS-19 [67] for video instance segmentation. YouTube-VIS-19 consists of 2,883 high-resolution YouTube videos and each video usually contains multiple object instances of distinct semantics. During the inference, we evaluate our method on two lines of tasks:

Unsupervised Single Object Segmentation: We utilize DAVIS-16 [48], SegTrack-v2 [32], and FMBS-59 [44] datasets. Following the standard protocol [68], we merge all individual masks into one unified foreground mask for SegTrack-v2 and FMBS-59, reporting the mean Intersection over Union (mIoU) on the validation set. Note that the evaluation is in the *zero-shot* manner, as the model does not see the whole dataset before testing.

Unsupervised Multiple Object Segmentation: We use the synthetic MOVi-E [19] dataset and real-world datasets like DAVIS-17-Unsupervised [50] and YouTube-VIS-19 [67], reporting Foreground Adjusted Rand Index (FG-ARI) and mIoU. For MOVi-E, we integrate its training set into our training due to significant distribution shifts. For the rest, we maintain solely training on the YouTube-VIS-19 set.

4.2. Implementation Details

In training, we sample $T = 3$ frames with temporal stride 4 as the input clip. Each frame is augmented with random crop and color jitter, and resized to 192×384 . We adopt DINO pretrained ViT-S/8 [7] as the frame encoder, which is then followed by a single spatio-temporal Transformer Encoder block with 8 heads as temporal correlator Φ_{st} . We set the number of sampled positive and negative pairs to $K_p = 10$ and $K_n = 50$ in default. For optimization, we adopt AdamW [40] with a learning rate 1×10^{-4} , and train the model for a total of 30k iterations with a batch size of 16. In the inference stage, our model can be flexibly applied to video sequences of arbitrary lengths. For the task of multi-object segmentation, we set the distance threshold in hierarchical clustering to 1.0. We follow the standard evaluation protocol outlined in the DAVIS-17 challenge [50] to match the predicted masks with the ground truth. In benchmarks for single object segmentation, where all objects are annotated as a whole, we adjust the distance threshold to 0.6 in order to merge all foreground objects into a single cluster.

4.3. Ablation Study

In the ablation study, we utilize DINO ViT-S/8 as the frozen backbone. We report FG-ARI and IoU on YouTube-VIS-2019 and \mathcal{J} & \mathcal{F} on DAVIS-17-Unsupervised for multi-object segmentation. For additional ablation studies, please refer to the appendix.

\mathcal{L}_s	\mathcal{L}_m	w	YTVIS-19		DAVIS-17	
			FG-ARI	mIoU	\mathcal{J} & \mathcal{F}	FG-ARI
-	-	-	23.4	25.5	23.1	18.4
✓	✗	✓	30.1	32.4	29.6	27.5
✗	✓	✓	39.9	46.1	38.6	37.3
✓	✓	✓	44.3	50.1	43.9	40.1
✓	✓	✗	43.1	48.1	42.5	38.1

Table 2. Ablation on different combinations of semantic consistency loss \mathcal{L}_s , motion consistency loss \mathcal{L}_m and entropy weight w . The first row represents the results obtained from a randomly initialized spatio-temporal Transformer block. Dynamic motion alignment plays a more fundamental role in our pixel-level segmentation tasks compared to semantic constraints. Besides, entropy normalization indeed refines the training process and yields superior results.

Clustering Metric	YTVIS-19		DAVIS-17	
	FG-ARI	mIoU	\mathcal{J} & \mathcal{F}	FG-ARI
F	22.1	23.8	16.1	19.4
F_v	33.9	31.4	33.4	32.1
A	30.1	34.8	29.3	30.5
A_v	44.3	50.1	43.9	40.1

Table 3. Ablation on different clustering metrics. Features F and attention maps A are directly obtained from DINO. F_v and A_v are generated from our learned spatio-temporal Transformer block. Either the attention map A from DINO or our spatio-temporal attention map A_v can serve as a more effective cue for clustering compared to their corresponding feature.

Training objective \mathcal{L}_s , \mathcal{L}_m , and w . To understand the contribution of each component to the VOS performance, we individually evaluate each loss item as depicted in Table 2. Compared to the baseline without training, the inclusion of semantic consistency loss \mathcal{L}_s with entropy-based weighting mechanism w (second row) elevates FG-ARI from 23.4 to 30.1 on YouTube-VIS-19. Furthermore, the motion consistency loss \mathcal{L}_m (third row) yields even more substantial improvements, resulting in FG-ARI reaching 39.9. This echos with our preliminary observations that the dynamic motions, as a manifestation of spatio-temporal dependencies, plays a more significant role than semantics in fine-grained object segmentation. Combining all components (fourth row) provides the best results, highlighting the synergy between the components. Additionally, removing the weighting function w (fifth row) slightly decreases the performance on both two benchmarks, affirming the necessity of entropy normalization to prioritize informative regions.

Clustering metrics. To further explore whether our clustering strategy optimally leverages the learned spatio-temporal properties, we select four types of clustering metrics for

		YTVIS-19		DAVIS-17	
T	Stride	FG-ARI	mIoU	\mathcal{J} & \mathcal{F}	FG-ARI
3	1	37.4	43.6	37.1	33.6
3	4	44.3	50.1	43.9	40.1
3	8	44.2	50.2	43.3	40.7
5	4	44.8	50.6	44.3	41.5

Table 4. Ablation on the number of frames T and temporal stride. When sampling more than 3 frames with a larger stride, the method starts to exhibit a diminishing effect.

comparison. Specifically, we adopt both feature vectors and attention maps directly from DINO and those from our learned spatio-temporal Transformer block. Table 3 reveals two key observations. First, our learning paradigm consistently outperforms the off-the-shelf DINO in terms of both features and attention maps, improving all metrics by over 10 points. This strongly supports our motivation that establishing spatio-temporal correspondence is crucial for video object segmentation. Second, utilizing the intermediate attention maps directly for clustering proves to be more effective than employing the final features. We speculate this occurs because the attention maps encode fine-grained structural dependencies between various positions, whereas feature vectors primarily capture high-level semantics.

Number of frames T and temporal stride. To investigate whether a wider temporal receptive field can reinforce temporal coherence and enhance object segmentations, we experiment by varying the number of input frames and temporal stride in training. Our results, displayed in Table 4, reveal that the performance significantly deteriorates when the stride is very small, such as a temporal stride of 1 in the first row. However, it begins to plateau upon reaching 4. This is because a small temporal stride leads to very subtle temporal dynamics in consecutive frames, resulting in a trivial learning task while a larger temporal stride provides richer dynamics, effectively encouraging the model to capture temporal consistency and maintain object permanence. Besides, introducing more frames leads to slight improvement. This phenomenon suggests that a modest temporal receptive field can provide sufficient temporal context for video object segmentation.

4.4. Comparison with State-of-the-art

Unsupervised Single Object Segmentation. We first present the quantitative results on unsupervised single object discovery in Table 5. Note that all the compared methods are trained on the target dataset, while our model is only trianed on YouTube-VIS-19 and directly transferred to these single object segmentation benchmarks in a *zero-shot* manner. Despite this, our method still achieves the best performance among those only using RGB data. Though

Model	RGB	Flow	DAVIS	ST-v2	FBMS
NLC [16]	✓	✓	55.1	67.2	51.5
CIS [68]	✓	✓	59.2	45.6	36.8
TokenCut [62]	✓	✓	64.3	60.2	59.6
MOD [12]	✓	✓	73.9	62.2	61.3
DyStaB [69]	✓	✓	80.0	74.2	73.2
DeSprite [71]	✓	✓	79.1	72.1	71.8
RCF [37]	✓	✓	80.9	76.7	69.9
SIMO [31]	✗	✓	67.8	62.0	-
MG [66]	✗	✓	68.3	58.6	53.1
EM [43]	✗	✓	69.3	55.5	57.8
OCLR [64]	✗	✓	72.1	67.6	65.4
AMD [38]	✓	✗	57.8	57.0	47.5
SMTC [53]	✓	✗	71.8	69.3	68.4
Ours	✓	✗	75.4	74.8	73.3

Table 5. Quantitative results on single object video segmentation. The tick(✓) and cross(✗) labels under the RGB and Flow columns indicate whether a method utilizes the corresponding modality during training or inference. We compare per frame mean IoU on DAVIS-16, SegTrack-v2 and FBMS-59 without any post-processing (e.g., spectral clustering, test-time adaptation, CRF [28]).

SMTC [53] proposes a sophisticated VOS framework based on slot attention, our method outperforms it by approximately 5 points. The superiority demonstrates the generalization ability of our approach simply guided by attention. As for the counterparts that resort to optical flow, some of them achieve very promising performance on three benchmarks [37, 70, 71]. This is because optical flow provides strong prior in highlighting the moving areas in videos, which well aligns with the single object segmentation task. However, optical flow can be challenging to obtain and may be unreliable, especially in complex scenes. In contrast, our method does not require any additional data modalities and can be flexibly extended to various scenarios.

Unsupervised Multiple Object Segmentation. We also evaluate our method on more challenging multi-object segmentation, which aims to segment different objects in a temporally coherent manner. Among the compared methods, SAVi [27] and OCLR [64] employ optical flow as supervision to discriminate motions of different objects. STEVE [57], VideoSAUR [73], SOLV [1] and SMTC [53] develop variants of slot attention with temporal constraints to bind to distinct instances. TimeT [54] propagates dense DINO features across time to enhance temporal consistency and applies clustering on learned features to produce object segmentations. In contrast, our method directly uses spatio-temporal attention maps for object segmentation. As shown in Table 6, our method achieves state-of-the-art results on both synthetic (MOVi-E) and realistic video dataset (YTVIS-19 and DAVIS-17), indicating the promis-

Model	MOV-E		YTVIS-19		DAVIS-17			
	FG-ARI	mIoU	FG-ARI	mIoU	FG-ARI	$\mathcal{J} \& \mathcal{F}$	\mathcal{J}	\mathcal{F}
SAVi [27]	42.8	16.0	11.1	12.7	-	-	-	-
STEVE [57]	50.6	26.6	20.0	20.9	-	-	-	-
OCLR [64]	-	-	15.9	32.5	14.7	-	34.6	-
VideoSAUR [73]	73.9	35.6	39.5	29.1	-	-	-	-
SOLV [1]	80.8	-	29.1	45.3	32.2	-	30.2	-
SMTCA [53]	-	-	31.4	38.8	33.3	40.5	36.4	44.6
TimeT* [54]	-	-	37.9	40.4	35.5	40.0	35.8	44.2
Ours	83.4	40.2	44.3	50.1	40.1	43.9	39.2	48.6
Ours [†]	84.4	40.7	44.5	50.1	41.6	43.7	39.4	48.0

Table 6. Quantitative results on multiple object video segmentation. For MOV-E and YouTube-VIS-19 datasets, we report FG-ARI and mIoU. Besides, we report Region Similarity \mathcal{J} and Contour Accuracy \mathcal{F} on DAVIS-17-Unsupervised. * The original paper of TimeT [54] includes the IoU of background category, we rerun the evaluation to exclude background here. † We use DINOv2 ViT-S/14 as our frozen frame encoder.

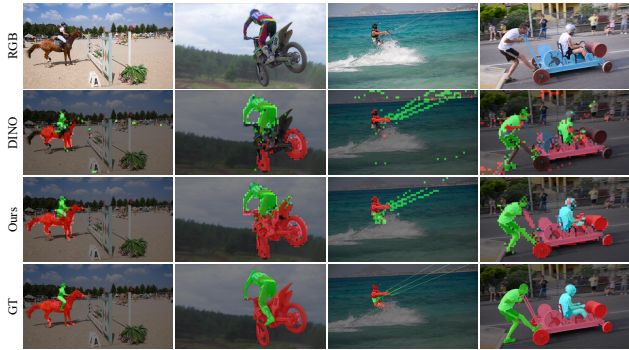


Figure 3. Qualitative comparison with DINO baseline on DAVIS-17-Unsupervised. Different color denotes different clusters.

ing generalization ability. Specifically, comparing to the prior arts, we gain an approximately 5-point advantage over both VideoSAUR [73] on YTVIS-19 and SMTCA [53] and TimeT [54] on DAVIS-17 in terms of FG-ARI. The superior results under our simple architecture reveal the feasibility of utilizing the spatio-temporal dependencies to mine object cues and derive reliable video object segmentation results. Besides, we also report the results using DINOv2 ViT-S/14 as the frame encoder. Despite the larger patch size, our method still achieves competitive performance. This demonstrates the robustness of our approach with respect to pretraining models.

Qualitative Comparison. To visually demonstrate the effectiveness of our proposed method, we contrast our segmentation results with those of the DINO counterpart in Fig. 3. For the DINO baseline, we cluster the patches through the attention map A . As can be observed, our method is able to segment with significantly less noise compared to DINO. For instance, in the motocross-jump se-

quence, our method nearly outlines the entire motorbike and the rider, whereas DINO misses most of the bike's body and only identifies its tyre. This shows that inferring the masks by associating a collection of RGB features and constructing spatio-temporal correspondences greatly enhances the segmentation result. Additionally, with the benefit of temporal correspondence, our model can differentiate between distinct object instances with the same semantics. Consider the soapbox sequence displayed in the right column; our method distinguishes two different people - one running behind the soapbox and another sitting in the soapbox throughout the video. This level of distinction cannot be obtained from DINO's spatial attention map, further emphasizing the effectiveness of introducing rich spatio-temporal relations in video segmentation tasks.

5. Conclusion

In this paper, we introduce a simple yet powerful approach for self-supervised video object segmentation. Specifically, our proposed architecture includes only a single spatio-temporal Transformer block that ingests frame-wise DINO features and constructs the spatio-temporal correspondence through the attention layer. During training, we adopt a dual self-supervised consistency objective that encompasses both semantic consistency and dynamic motion consistency, supplemented with entropy normalization. In inference, we utilize hierarchical clustering on spatio-temporal attention maps to generate temporally coherent object segmentation masks. This extremely straightforward approach nevertheless delivers state-of-the-art results across many VOS benchmarks, including exceptional performance on challenging real-world multi-object segmentation tasks such as DAVIS-17-Unsupervised and YouTube-VIS-19.

References

[1] Görkay Aydemir, Weidi Xie, and Fatma Guney. Self-supervised object-centric learning for videos. In *Thirty-seventh Conference on Neural Information Processing Systems*, 2023. 2, 3, 7, 8, 1

[2] Linchao Bao, Baoyuan Wu, and Wei Liu. Cnn in mrf: Video object segmentation via inference in a cnn-based higher-order spatio-temporal mrf. In *Proceedings of the IEEE conference on computer vision and pattern recognition*, pages 5977–5986, 2018. 2

[3] Gedas Bertasius, Heng Wang, and Lorenzo Torresani. Is space-time attention all you need for video understanding? In *ICML*, page 4, 2021. 4

[4] Zhangxing Bian, Allan Jabri, Alexei A Efros, and Andrew Owens. Learning pixel trajectories with multiscale contrastive random walks. In *Proceedings of the IEEE/CVF Conference on Computer Vision and Pattern Recognition*, pages 6508–6519, 2022. 3

[5] Adam Bielski and Paolo Favaro. Move: Unsupervised movable object segmentation and detection. *Advances in Neural Information Processing Systems*, 35:33371–33386, 2022. 3

[6] Sergi Caelles, Kevis-Kokitsi Maninis, Jordi Pont-Tuset, Laura Leal-Taixé, Daniel Cremers, and Luc Van Gool. One-shot video object segmentation. In *Proceedings of the IEEE conference on computer vision and pattern recognition*, pages 221–230, 2017. 2

[7] Mathilde Caron, Hugo Touvron, Ishan Misra, Hervé Jégou, Julien Mairal, Piotr Bojanowski, and Armand Joulin. Emerging properties in self-supervised vision transformers. In *Proceedings of the IEEE/CVF International Conference on Computer Vision*, pages 9650–9660, 2021. 2, 3, 4, 6

[8] Ting Chen, Simon Kornblith, Mohammad Norouzi, and Geoffrey Hinton. A simple framework for contrastive learning of visual representations. In *International conference on machine learning*, pages 1597–1607. PMLR, 2020. 2

[9] Subhabrata Choudhury, Laurynas Karazija, Iro Laina, Andrea Vedaldi, and Christian Rupprecht. Guess What Moves: Unsupervised Video and Image Segmentation by Anticipating Motion. In *British Machine Vision Conference (BMVC)*, 2022. 2

[10] Shuangrui Ding, Maomao Li, Tianyu Yang, Rui Qian, Haohang Xu, Qingyi Chen, Jue Wang, and Hongkai Xiong. Motion-aware contrastive video representation learning via foreground-background merging. In *Proceedings of the IEEE/CVF Conference on Computer Vision and Pattern Recognition*, pages 9716–9726, 2022. 2

[11] Shuangrui Ding, Rui Qian, and Hongkai Xiong. Dual contrastive learning for spatio-temporal representation. In *Proceedings of the 30th ACM International Conference on Multimedia*, pages 5649–5658, 2022. 2

[12] Shuangrui Ding, Weidi Xie, Yabo Chen, Rui Qian, Xiaopeng Zhang, Hongkai Xiong, and Qi Tian. Motion-inductive self-supervised object discovery in videos. *arXiv preprint arXiv:2210.00221*, 2022. 7

[13] Alexey Dosovitskiy, Lucas Beyer, Alexander Kolesnikov, Dirk Weissenborn, Xiaohua Zhai, Thomas Unterthiner, Mostafa Dehghani, Matthias Minderer, Georg Heigold, Sylvain Gelly, et al. An image is worth 16x16 words: Transformers for image recognition at scale. *arXiv preprint arXiv:2010.11929*, 2020. 2

[14] Suyog Dutt Jain, Bo Xiong, and Kristen Grauman. Fusionseg: Learning to combine motion and appearance for fully automatic segmentation of generic objects in videos. In *Proceedings of the IEEE conference on computer vision and pattern recognition*, pages 3664–3673, 2017. 2

[15] Gamaleldin Elsayed, Aravindh Mahendran, Sjoerd van Steenkiste, Klaus Greff, Michael C Mozer, and Thomas Kipf. Savi++: Towards end-to-end object-centric learning from real-world videos. *Advances in Neural Information Processing Systems*, 35:28940–28954, 2022. 2

[16] Alon Faktor and Michal Irani. Video segmentation by non-local consensus voting. In *BMVC*, page 8, 2014. 7

[17] Deng-Ping Fan, Wenguan Wang, Ming-Ming Cheng, and Jianbing Shen. Shifting more attention to video salient object detection. In *Proceedings of the IEEE/CVF conference on computer vision and pattern recognition*, pages 8554–8564, 2019. 2

[18] Di Feng, Christian Haase-Schütz, Lars Rosenbaum, Heinz Hertlein, Claudius Glaeser, Fabian Timm, Werner Wiesbeck, and Klaus Dietmayer. Deep multi-modal object detection and semantic segmentation for autonomous driving: Datasets, methods, and challenges. *IEEE Transactions on Intelligent Transportation Systems*, 22(3):1341–1360, 2020. 2

[19] Klaus Greff, Francois Belletti, Lucas Beyer, Carl Doersch, Yilun Du, Daniel Duckworth, David J Fleet, Dan Gnanapragasam, Florian Golemo, Charles Herrmann, Thomas Kipf, Abhijit Kundu, Dmitry Lagun, Issam Laradji, Hsueh-Ti (Derek) Liu, Henning Meyer, Yishu Miao, Derek Nowrouzezahrai, Cengiz Oztireli, Etienne Pot, Noha Radwan, Daniel Rebain, Sara Sabour, Mehdi S. M. Sajjadi, Matan Sela, Vincent Sitzmann, Austin Stone, Deqing Sun, Suhani Vora, Ziyu Wang, Tianhao Wu, Kwang Moo Yi, Fangcheng Zhong, and Andrea Tagliasacchi. Kubric: a scalable dataset generator. 2022. 2, 6, 1

[20] Mark Hamilton, Zhoutong Zhang, Bharath Hariharan, Noah Snavely, and William T. Freeman. Unsupervised semantic segmentation by distilling feature correspondences. In *International Conference on Learning Representations*, 2022. 3

[21] Kaiming He, Haoqi Fan, Yuxin Wu, Saining Xie, and Ross Girshick. Momentum contrast for unsupervised visual representation learning. In *Proceedings of the IEEE/CVF conference on computer vision and pattern recognition*, pages 9729–9738, 2020. 2

[22] Yingdong Hu, Renhao Wang, Kaifeng Zhang, and Yang Gao. Semantic-aware fine-grained correspondence. In *European Conference on Computer Vision*, pages 97–115. Springer, 2022. 3

[23] Yuan-Ting Hu, Jia-Bin Huang, and Alexander G Schwing. Videomatch: Matching based video object segmentation. In *Proceedings of the European conference on computer vision (ECCV)*, pages 54–70, 2018. 2

[24] Allan Jabri, Andrew Owens, and Alexei Efros. Space-time correspondence as a contrastive random walk. *Advances in neural information processing systems*, 33:19545–19560, 2020. 3

[25] Joakim Johnander, Martin Danelljan, Emil Brissman, Fahad Shahbaz Khan, and Michael Felsberg. A generative appearance model for end-to-end video object segmentation. In *Proceedings of the IEEE/CVF Conference on Computer Vision and Pattern Recognition*, pages 8953–8962, 2019. 2

[26] Stephen C Johnson. Hierarchical clustering schemes. *Psychometrika*, 32(3):241–254, 1967. 2, 4

[27] Thomas Kipf, Gamaleldin Fathy Elsayed, Aravindh Mahendran, Austin Stone, Sara Sabour, Georg Heigold, Rico Jonschkowski, Alexey Dosovitskiy, and Klaus Greff. Conditional object-centric learning from video. In *International Conference on Learning Representations*, 2022. 2, 7, 8

[28] John Lafferty, Andrew McCallum, and Fernando CN Pereira. Conditional random fields: Probabilistic models for segmenting and labeling sequence data. 2001. 7

[29] Z. Lai and W. Xie. Self-supervised learning for video correspondence flow. In *BMVC*, 2019. 2, 3

[30] Zihang Lai, Erika Lu, and Weidi Xie. Mast: A memory-augmented self-supervised tracker. In *Proceedings of the IEEE/CVF Conference on Computer Vision and Pattern Recognition*, pages 6479–6488, 2020. 3

[31] Hala Lamdouar, Weidi Xie, and Andrew Zisserman. Segmenting invisible moving objects. In *British Machine Vision Association*, 2021. 7

[32] Fuxin Li, Taeyoung Kim, Ahmad Humayun, David Tsai, and James M Rehg. Video segmentation by tracking many figure-ground segments. In *Proceedings of the IEEE international conference on computer vision*, pages 2192–2199, 2013. 2, 6, 1

[33] Liulei Li, Wenguan Wang, Tianfei Zhou, Jianwu Li, and Yi Yang. Unified mask embedding and correspondence learning for self-supervised video segmentation. In *Proceedings of the IEEE/CVF Conference on Computer Vision and Pattern Recognition*, pages 18706–18716, 2023. 3

[34] Xiaoxiao Li and Chen Change Loy. Video object segmentation with joint re-identification and attention-aware mask propagation. In *Proceedings of the European conference on computer vision (ECCV)*, pages 90–105, 2018. 2

[35] Xuetong Li, Sifei Liu, Shalini De Mello, Xiaolong Wang, Jan Kautz, and Ming-Hsuan Yang. Joint-task self-supervised learning for temporal correspondence. In *Advances in Neural Information Processing Systems*. Curran Associates, Inc., 2019. 2

[36] Xuetong Li, Sifei Liu, Shalini De Mello, Xiaolong Wang, Jan Kautz, and Ming-Hsuan Yang. Joint-task self-supervised learning for temporal correspondence. *Advances in Neural Information Processing Systems*, 32, 2019. 3

[37] Long Lian, Zhirong Wu, and Stella X Yu. Bootstrapping objectness from videos by relaxed common fate and visual grouping. In *Proceedings of the IEEE/CVF Conference on Computer Vision and Pattern Recognition*, pages 14582–14591, 2023. 2, 7

[38] Runtao Liu, Zhirong Wu, Stella Yu, and Stephen Lin. The emergence of objectness: Learning zero-shot segmentation from videos. In *Advances in Neural Information Processing Systems*, pages 13137–13152. Curran Associates, Inc., 2021. 2, 7

[39] Francesco Locatello, Dirk Weissenborn, Thomas Unterthiner, Aravindh Mahendran, Georg Heigold, Jakob Uszkoreit, Alexey Dosovitskiy, and Thomas Kipf. Object-centric learning with slot attention. *Advances in Neural Information Processing Systems*, 33:11525–11538, 2020. 2, 3

[40] Ilya Loshchilov and Frank Hutter. Decoupled weight decay regularization. In *International Conference on Learning Representations*, 2018. 6

[41] K-K Maninis, Sergi Caelles, Yuhua Chen, Jordi Pont-Tuset, Laura Leal-Taixé, Daniel Cremers, and Luc Van Gool. Video object segmentation without temporal information. *IEEE transactions on pattern analysis and machine intelligence*, 41(6):1515–1530, 2018. 2

[42] Luke Melas-Kyriazi, Christian Rupprecht, Iro Laina, and Andrea Vedaldi. Deep spectral methods: A surprisingly strong baseline for unsupervised semantic segmentation and localization. In *Proceedings of the IEEE/CVF Conference on Computer Vision and Pattern Recognition*, pages 8364–8375, 2022. 3

[43] Etienne Meunier, Anaïs Badoual, and Patrick Bouthemy. Em-driven unsupervised learning for efficient motion segmentation. *IEEE Transactions on Pattern Analysis and Machine Intelligence*, 45(4):4462–4473, 2022. 7

[44] Peter Ochs, Jitendra Malik, and Thomas Brox. Segmentation of moving objects by long term video analysis. *IEEE transactions on pattern analysis and machine intelligence*, 36(6):1187–1200, 2013. 2, 6, 1

[45] Seoung Wug Oh, Joon-Young Lee, Ning Xu, and Seon Joo Kim. Video object segmentation using space-time memory networks. In *Proceedings of the IEEE/CVF International Conference on Computer Vision*, pages 9226–9235, 2019. 2

[46] Maxime Oquab, Timothée Darcret, Théo Moutakanni, Huy Vo, Marc Szafraniec, Vasil Khalidov, Pierre Fernandez, Daniel Haziza, Francisco Massa, Alaaeldin El-Nouby, et al. Dinov2: Learning robust visual features without supervision. *arXiv preprint arXiv:2304.07193*, 2023. 2

[47] Prashant W Patil, Akshay Duhane, Ashutosh Kulkarni, Subrahmanyam Murala, Anil Balaji Gonde, and Sunil Gupta. An unified recurrent video object segmentation framework for various surveillance environments. *IEEE Transactions on Image Processing*, 30:7889–7902, 2021. 2

[48] Federico Perazzi, Jordi Pont-Tuset, Brian McWilliams, Luc Van Gool, Markus Gross, and Alexander Sorkine-Hornung. A benchmark dataset and evaluation methodology for video object segmentation. In *Proceedings of the IEEE conference on computer vision and pattern recognition*, pages 724–732, 2016. 2, 4, 6, 1

[49] Federico Perazzi, Anna Khoreva, Rodrigo Benenson, Bernt Schiele, and Alexander Sorkine-Hornung. Learning video object segmentation from static images. In *Proceedings of the IEEE conference on computer vision and pattern recognition*, pages 2663–2672, 2017. 2

[50] Jordi Pont-Tuset, Federico Perazzi, Sergi Caelles, Pablo Arbeláez, Alex Sorkine-Hornung, and Luc Van Gool. The 2017

davis challenge on video object segmentation. *arXiv preprint arXiv:1704.00675*, 2017. 2, 4, 6, 1

[51] Rui Qian, Yuxi Li, Huabin Liu, John See, Shuangrui Ding, Xian Liu, Dian Li, and Weiyao Lin. Enhancing self-supervised video representation learning via multi-level feature optimization. In *Proceedings of the IEEE/CVF international conference on computer vision*, pages 7990–8001, 2021. 2

[52] Rui Qian, Shuangrui Ding, Xian Liu, and Dahua Lin. Static and dynamic concepts for self-supervised video representation learning. In *European Conference on Computer Vision*, pages 145–164. Springer, 2022. 2

[53] Rui Qian, Shuangrui Ding, Xian Liu, and Dahua Lin. Semantics meets temporal correspondence: Self-supervised object-centric learning in videos. In *Proceedings of the IEEE/CVF International Conference on Computer Vision*, pages 16675–16687, 2023. 2, 3, 7, 8

[54] Mohammadreza Salehi, Efstratios Gavves, Cees GM Snoek, and Yuki M Asano. Time does tell: Self-supervised time-tuning of dense image representations. In *Proceedings of the IEEE/CVF International Conference on Computer Vision*, pages 16536–16547, 2023. 2, 3, 7, 8

[55] Jianbo Shi and Jitendra Malik. Normalized cuts and image segmentation. *IEEE Transactions on pattern analysis and machine intelligence*, 22(8):888–905, 2000. 3

[56] Oriane Siméoni, Gilles Puy, Huy V Vo, Simon Roburin, Spyros Gidaris, Andrei Bursuc, Patrick Pérez, Renaud Marlet, and Jean Ponce. Localizing objects with self-supervised transformers and no labels. In *BMVC 2021-32nd British Machine Vision Conference*, 2021. 3

[57] Gautam Singh, Yi-Fu Wu, and Sungjin Ahn. Simple unsupervised object-centric learning for complex and naturalistic videos. *Advances in Neural Information Processing Systems*, 35:18181–18196, 2022. 7, 8

[58] Carl Vondrick, Abhinav Shrivastava, Alireza Fathi, Sergio Guadarrama, and Kevin Murphy. Tracking emerges by colorizing videos. In *Proceedings of the European conference on computer vision (ECCV)*, pages 391–408, 2018. 3

[59] Ning Wang, Yibing Song, Chao Ma, Wengang Zhou, Wei Liu, and Houqiang Li. Unsupervised deep tracking. In *Proceedings of the IEEE/CVF Conference on Computer Vision and Pattern Recognition*, pages 1308–1317, 2019. 2

[60] Xiaolong Wang, Allan Jabri, and Alexei A Efros. Learning correspondence from the cycle-consistency of time. In *Proceedings of the IEEE/CVF Conference on Computer Vision and Pattern Recognition*, pages 2566–2576, 2019. 3

[61] Xudong Wang, Rohit Girdhar, Stella X. Yu, and Ishan Misra. Cut and learn for unsupervised object detection and instance segmentation. In *Proceedings of the IEEE/CVF Conference on Computer Vision and Pattern Recognition (CVPR)*, pages 3124–3134, 2023. 3

[62] Yangtao Wang, Xi Shen, Yuan Yuan, Yuming Du, Maomao Li, Shell Xu Hu, James L Crowley, and Dominique Vaufreydaz. Tokencut: Segmenting objects in images and videos with self-supervised transformer and normalized cut. *IEEE Transactions on Pattern Analysis and Machine Intelligence*, 2023. 3, 7

[63] Christopher Xie, Yu Xiang, Zaid Harchaoui, and Dieter Fox. Object discovery in videos as foreground motion clustering. In *Proceedings of the IEEE/CVF Conference on Computer Vision and Pattern Recognition*, pages 9994–10003, 2019. 2

[64] Junyu Xie, Weidi Xie, and Andrew Zisserman. Segmenting moving objects via an object-centric layered representation. In *Advances in Neural Information Processing Systems*, 2022. 2, 3, 7, 8, 1

[65] Jiarui Xu and Xiaolong Wang. Rethinking self-supervised correspondence learning: A video frame-level similarity perspective. In *Proceedings of the IEEE/CVF International Conference on Computer Vision*, pages 10075–10085, 2021. 3

[66] Charig Yang, Hala Lamdouar, Erika Lu, Andrew Zisserman, and Weidi Xie. Self-supervised video object segmentation by motion grouping. In *Proceedings of the IEEE/CVF International Conference on Computer Vision (ICCV)*, pages 7177–7188, 2021. 2, 7

[67] Linjie Yang, Yuchen Fan, and Ning Xu. Video instance segmentation. In *ICCV*, 2019. 2, 6, 1

[68] Yanchao Yang, Antonio Loquercio, Davide Scaramuzza, and Stefano Soatto. Unsupervised moving object detection via contextual information separation. In *Proceedings of the IEEE/CVF Conference on Computer Vision and Pattern Recognition (CVPR)*, 2019. 2, 6, 7, 1

[69] Yanchao Yang, Brian Lai, and Stefano Soatto. Dystab: Unsupervised object segmentation via dynamic-static bootstrapping. In *Proceedings of the IEEE/CVF Conference on Computer Vision and Pattern Recognition (CVPR)*, pages 2826–2836, 2021. 2, 7

[70] Yanchao Yang, Brian Lai, and Stefano Soatto. Dystab: Unsupervised object segmentation via dynamic-static bootstrapping. In *Proceedings of the IEEE/CVF Conference on Computer Vision and Pattern Recognition*, pages 2826–2836, 2021. 7

[71] Vickie Ye, Zhengqi Li, Richard Tucker, Angjoo Kanazawa, and Noah Snavely. Deformable sprites for unsupervised video decomposition. In *Proceedings of the IEEE/CVF Conference on Computer Vision and Pattern Recognition*, pages 2657–2666, 2022. 2, 7

[72] Andrii Zadaianchuk, Matthaeus Kleindessner, Yi Zhu, Francesco Locatello, and Thomas Brox. Unsupervised semantic segmentation with self-supervised object-centric representations. In *The Eleventh International Conference on Learning Representations*, 2023. 3

[73] Andrii Zadaianchuk, Maximilian Seitzer, and Georg Martius. Object-centric learning for real-world videos by predicting temporal feature similarities. In *Thirty-seventh Conference on Neural Information Processing Systems (NeurIPS 2023)*, 2023. 2, 7, 8, 1

[74] Adrian Ziegler and Yuki M Asano. Self-supervised learning of object parts for semantic segmentation. In *Proceedings of the IEEE/CVF Conference on Computer Vision and Pattern Recognition*, pages 14502–14511, 2022. 3

Betrayed by Attention: A Simple yet Effective Approach for Self-supervised Video Object Segmentation

Supplementary Material

A. More Implementation Details

Dataset. Firstly, we benchmark on three popular datasets designed for single object segmentation. **DAVIS-16** [48] consists of 50 high quality videos, 3455 frames in total. Every frame is annotated with a pixel-level accurate segmentation mask. **SegTrack-v2** [32] contains 14 sequences and 947 fully-annotated frames. Each sequence involves 1-6 moving objects and presents challenges including motion blur, appearance change, complex deformation, occlusion, slow motion, and interacting objects. **FBMS-59** [44] has 59 sequences with greatly varied resolution and annotates every 20th frame. Many sequences contain multiple moving objects. Following previous evaluation metric [64, 68], we merge objects of SegTrackv2 and FBMS-59 into a single one for video object segmentation. We calculate the mean per-frame the Jaccard Index \mathcal{J} over the validation set.

For multi-object segmentation in video, we evaluate our method on one synthetic and two real-world video datasets. **MOVi-E** [19] dataset is a synthetic dataset with granular control over data complexity and comprehensive ground truth annotations. MOVi-E scenes contain up to 23 objects and introduce simple linear camera movement. Our evaluation of learned features extends to real-world datasets **DAVIS-17** [50] and **YouTube-VIS-19** [67]. DAVIS-17, an expansion of DAVIS-16, includes 40 additional video sequences along with multi-object segmentation annotations. We utilize 30 validation videos on DAVIS-2017 for evaluation. As for YouTube-VIS-19, due to the lack of mask annotations in the validation or test set, following previous works [1, 73], we select 300 out of the whole 2,883 videos in training set for evaluation. For MOVi-E and YouTube-VIS-19, we report the Foreground Adjusted Rand Index (FG-ARI) and mean Intersection over Union (mIoU). Furthermore, for DAVIS-2017, we adhere to the standard protocol [50] and report both Region Similarity (\mathcal{J}) and Contour Accuracy (\mathcal{F}).

Hierarchical Clustering Algorithm. We present our Hierarchical Clustering based inference in Alg. 1. Given the spatio-temporal attention maps $A_v \in \mathbb{R}^{THW \times THW}$, the algorithm finally outputs the cluster centers $A_c \in \mathbb{R}^{K \times THW}$ and cluster assignments $Z \in \{1, \dots, K\}^{T'HW}$ which serve as predicted object segmentation masks. Specifically, each attention map is treated as a separate cluster. The process then cycles through each attention map (or current ‘cluster’), calculating distances between it and all other clusters using the KL-divergence metric. It identifies the clusters

Model	YTVIS-19		DAVIS-17	
	FG-ARI	mIoU	$\mathcal{J} \& \mathcal{F}$	FG-ARI
DINO ViT-S/16	42.5	47.2	41.7	38.3
DINO ViT-S/8	44.3	50.1	43.9	40.1
DINO ViT-B/8	43.5	50.2	42.8	40.7
DINOv2 ViT-S/14	44.1	49.7	43.1	40.5
DINOv2 ViT-B/14	44.5	50.1	43.7	41.6

Table 7. Ablation on different pretrained backbones. We show the results on various DINO and DINOv2 pretrained ViT encoders with different patch sizes.

that are close to it (i.e., those whose distance is less than the threshold) and combines them to form a new, larger cluster, represented by their updated centroid. This updated cluster set then replaces the initial set of attention maps, and the process continues iteratively until no more clusters can be merged. Finally, the algorithm assigns each original attention map to the cluster whose center it is closest to, yielding the final cluster assignments. Note that executing inference on extensive video sequences with a large T value might cause the self-attention matrix to become redundant, thereby requiring significant computational resources. To address this limitation, we sparsely sample T' frames ($T' \ll T$) as *key*, with the original densely sampled frames as *query*, and calculate the cross-attention $A'_v \in \mathbb{R}^{THW \times T'HW}$. By applying clustering to more compact A'_v , we linearly reduce memory requirements and maintain stable performance as shown in Sec. B.

B. More Ablation Study

Pretrained backbones. We present the ablation studies on different pretrained backbones in Table. 7. We show the results on both DINO and DINOv2 pretrained ViT encoders with different patch sizes. Generally, our method achieves competitive results on all variants of visual encoders. Comparing the first two lines, i.e., DINO ViT-S/16 vs. DINO ViT-S/8, smaller patch size contributes to notable performance improvements, approximately 2 points on two benchmarks, due to more fine-grained segmentation predictions. Comparing DINO and DINOv2, despite larger patch size, more advanced DINOv2 pretrained backbones reach comparable performance. This reveals the robustness and flexibility of our method to different backbones.

Motion representations. In training, we use the spatio-temporal attention maps as latent motion representations

Algorithm 1 Hierarchical Clustering

Input: Spatio-temporal attention maps $A_v \in \mathbb{R}^{THW \times T'HW}$, distance threshold τ
Output: Cluster assignment $Z \in \{1, \dots, K\}^{THW}$

Initialize cluster centers $A_c \leftarrow A_v$
while the number of clusters in A_c changes **do**
 Initialize updated clusters $A_p \leftarrow \{\}$
 for all $x \in A_c$ **do**
 Compute distances: $\mathcal{M} \leftarrow \text{calculate_distance}(x, A_c)$
 Identify proximal members: $\mathcal{I} \leftarrow \{i \mid \mathcal{M}[i] < \tau\}$
 Calculate new cluster centroid: $x \leftarrow \frac{1}{|\mathcal{I}|} \sum_{i \in \mathcal{I}} A_c[i]$
 Add new centroid to updated clusters: $A_p \leftarrow A_p \cup \{x\}$
 Remove merged attention maps from current cluster set: $A_c \leftarrow A_c \setminus A_c[i], \forall i \in \mathcal{I}$
 end for
 Update the clusters: $A_c \leftarrow A_p$
end while
Compute final distances: $\mathcal{M} \leftarrow \text{calculate_distance}(A_v, A_c)$
Compute final cluster assignments: $Z \leftarrow \text{argmin}(\mathcal{M}, \text{dim}=1)$

MotionRep	YTVIS-19		DAVIS-17		
	FG-ARI	mIoU	$\mathcal{J} \& \mathcal{F}$	FG-ARI	
Local Correlation	30.5	33.8	29.6	27.7	
Global Correlation	39.1	49.2	36.4	33.9	
Self-Attention	44.3	50.1	43.9	40.1	

Table 8. Ablation on different motion representations in calculating motion consistency loss \mathcal{L}_m . We compare using the self-attention matrix, simple local and global feature correlation as the latent motion representation.

for dynamic motion alignment \mathcal{L}_m . There are some alternatives to formulate this motion representation. Here we explore two variants in Table 8. The one is simple global feature correlation, which directly calculates the dot product between spatio-temporal feature vectors, i.e., $C_g = \tilde{F}\tilde{F}^T \in \mathbb{R}^{THW \times THW}$. The other is local feature correlation, where we sample a sliding local window with size $T_p \times H_p \times W_p$ for each grid, and obtain the local correlation matrix $C_l \in \mathbb{R}^{THW \times T_p H_p W_p}$. It is obvious that using the self-attention maps as motion representation substantially outperforms the performance of the other two methods. Compared to the global correlation, the learnable parameters in attention layers enhance the modeling capacity, which enables the self-attention maps to capture more comprehensive spatio-temporal dependencies and serve as a better motion representation. The local correlation only captures temporal dynamics in limited reception fields, restricting the ability for long-term perception.

Number of key frames. As stated in the above section, it is feasible to sparsely sample video frames as `key` to reduce computation costs in inference. We present the abla-

Ratio	YTVIS-19		DAVIS-17		Speed
	FG-ARI	mIoU	$\mathcal{J} \& \mathcal{F}$	FG-ARI	
0.1	43.5	49.7	42.8	40.0	2.3 \times
0.2	44.1	50.0	43.4	40.2	2.0 \times
0.5	44.3	50.2	43.8	40.1	1.4 \times
1.0	44.3	50.1	43.9	40.1	1.0 \times

Table 9. Ablation on different numbers of key frames sampled for calculating the spatio-temporal attention matrix. We compare performance under different ratios.

tion study in Table 9. We report the multiple object segmentation performance as well as the inference throughput ratio (including the whole feature extraction, attention calculation and clustering process). Interestingly, our findings suggest that promising results for video object segmentation can still be achieved even when only 10% of the frames are sampled. This sparse sampling approach leads to a remarkable 2.3 \times speedup in inference. For illustration, given a video with T frames, we uniformly sample $T' = 0.1T$ frames as `key`, with the original T frames as `query`, and calculate the cross-attention $A'_v \in \mathbb{R}^{THW \times T'HW}$. This linearly reduces the channel dimension of each attention map. Then we perform hierarchical clustering on these THW samples with reduced channel dimension and produce the cluster assignments (segmentation masks) for all frames within the video in one shot. The underlying reason is that video frames are highly redundant, sparse sampling could provide an abundant temporal reference for spatio-temporal dependency calculation. Hence, by sampling a small percentage of the entire video, we achieve comparable performance with a substantial reduction in computational cost, leading to faster inference speeds.

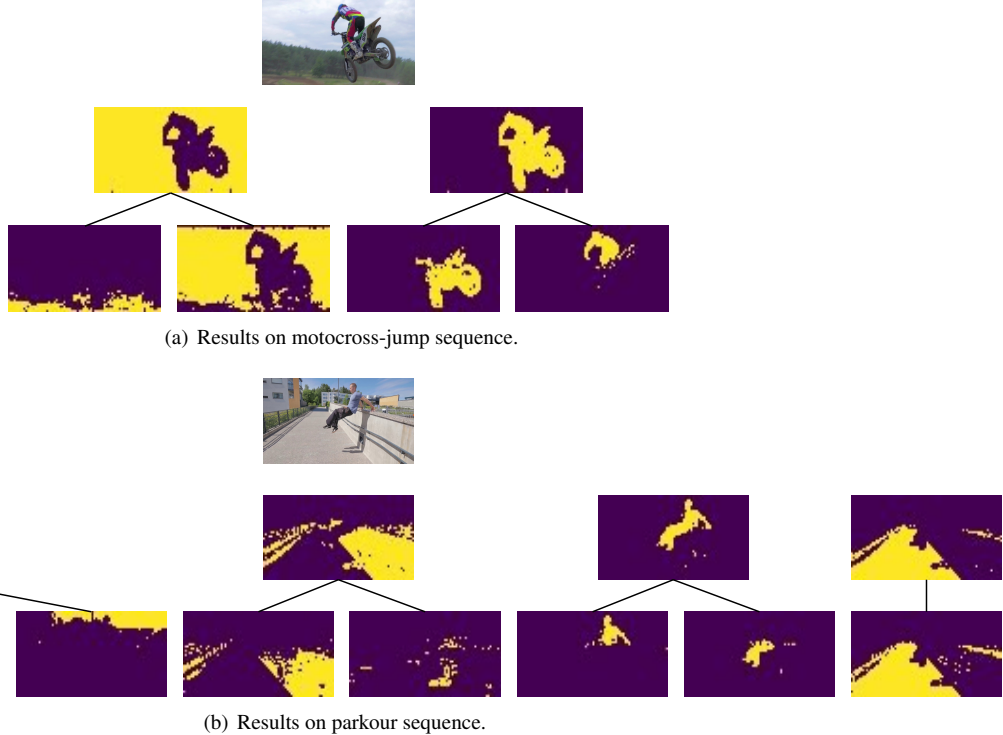


Figure 4. Visualization of the clustering process. We observe interpretable clustering hierarchies that segment objects at different granularities.

C. More Visualization Results

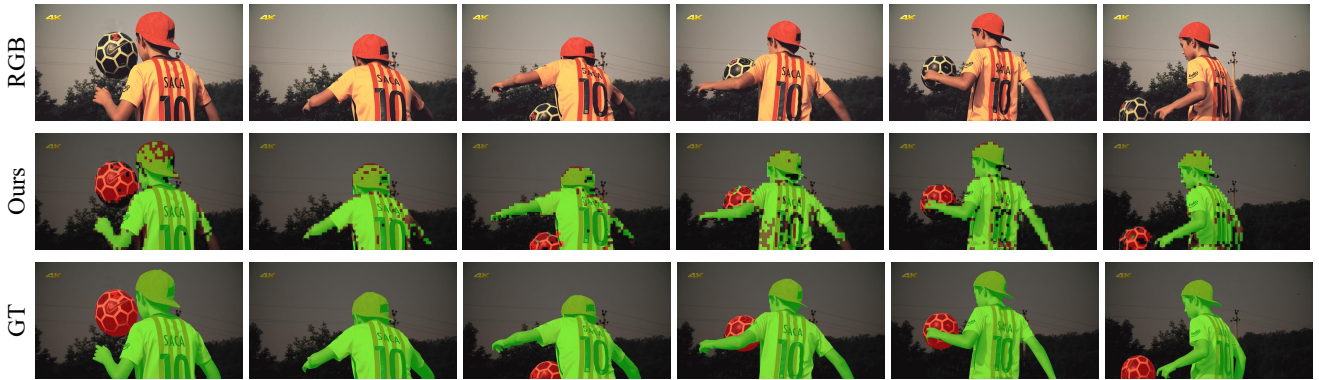
Results of different clustering hierarchies. In our inference stage, the hierarchical clustering algorithm produces different clustering hierarchies. We explore whether there exists an interpretable phenomenon during the clustering process in Fig. 4. Interestingly, we observe that our model is able to segment objects at different granularities across hierarchies. Generally, it results in more fine-grained object segmentation in lower hierarchies and vice versa. For example, in Fig. 4(a), the model discerns two distinct objects - the motorbike and the human - at a lower hierarchy, subsequently merging them into a cohesive foreground area at a higher hierarchy. Similarly, Fig. 4(b) shows that the clustering isolates different sections of the human figure at a lower hierarchy, before integrating them to form a holistic human body at a higher hierarchy. Such interpretable hierarchical clustering outcomes yield multi-layered object segmentations, potentially resolving the ambiguities in annotations.

Results on consecutive frames. We additionally show our segmentation results on video sequences with object occlusion, disappearance and reappearance, which is prevalent and challenging in real-world scenarios. In Fig. 5, we present three typical cases. The first is a cat-girl sequence, where there exist mutual occlusions between two objects.

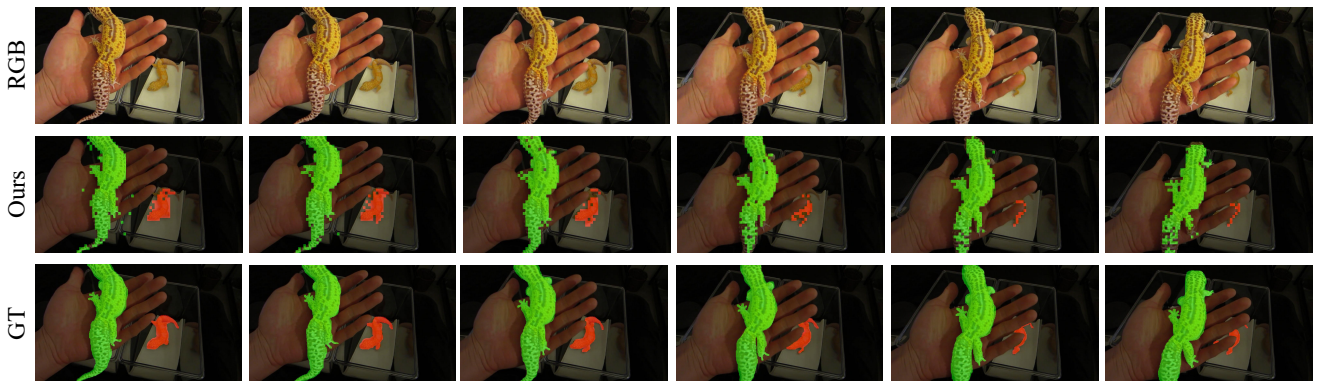
Our model is able to accurately segment the object parts despite severe occlusion. The second is a kid-football sequence, where the football disappears in the second frame and reappears in later frames. Since our method refers to the spatio-temporal dependencies across the whole temporal range, it is able to recognize that the ball in the first frame and those in later frames belong to the same instance. This enables our model to process real-world videos with complex temporal dynamics. The third is a very challenging sequence consisting of two lizards, which share very similar colors, body shapes and textures and only vary in sizes and positions. Moreover, the smaller one is severely occluded by the human hand in the latter three frames. Despite these challenges, our method is still able to distinguish these two lizards and accurately track specific instances over time. These examples demonstrate the applicability of our method to general video scenes.



(a) Results on cat-girl sequence.



(b) Results on kid-football sequence.



(c) Results on lizard sequence.

Figure 5. Visualization results on video sequences with occlusion. Our model is able to deal with partial or complete object occlusion, where an object disappears in some frame and reappears in later frames.